Microsystem Technologies (2024) 30:809–819
https://doi.org/10.1007/s00542-024-05658-3

REVIEW PAPER

CMOS-MEMS electrostatic micromotor based on FGMOS transduction by electromechanical modification of its coupling coefficient and low operating voltage

L. Sánchez–Márquez[1] · G. S. Abarca–Jiménez[2] · M. A. Reyes–Barranca[1] · J. Mares-Carreño[2]

Received: 7 December 2021 / Accepted: 25 March 2024 / Published online: 17 April 2024
© The Author(s), under exclusive licence to Springer-Verlag GmbH Germany, part of Springer Nature 2024

Abstract

This work consists of a design and simulation of a structure composed by an aluminum structural layer whose purpose is to act as an angular electrostatic micromotor. The structure of the micromotor is defined using the layers available from a 0.5 μm CMOS technology used for integrated circuit fabrication. In this proposal, a digital circuit is configured for the generation of the three phases needed for proper operation of the micromotor. The phases and poles of the stator are biased in an alternating sequence, thus, when there is a potential difference between the misaligned poles of the rotor and stator, an electrostatic force is generated that causes the motor to advance one step. If this sequence is performed correctly and periodically, the rotor reaches a set speed in a clockwise direction. As a novel contribution to the presented design, an FGMOS transistor is used as an auxiliary element to measure the rotating speed of the micromotor and whose control gate is a structure mechanically coupled to the rotor. The elements of the system are proposed for being monolithically integrated: the rotation control circuit, the micromotor, and the speed sensor. This work also shows a static simulation and a time-dependent simulation that allows predicting the behavior over time and the torque generated by the micro-actuator.

1 Introduction

Micromotors are actuators that generate movement due to some micro-activation force and can be fabricated based on MEMS dedicated technologies, like POLYMUMPS or METALMUMPS. The design of such MEMS micromotors has been explored for several years now (Fan et al. 1989; Mehregany et al. 1990), where the step-by-step motor configuration is preferred.

✉ M. A. Reyes–Barranca
mreyes@cinvestav.mx

L. Sánchez–Márquez
luis.sanchez.m@cinvestav.mx

G. S. Abarca–Jiménez
gabarcaj@ipn.mx

J. Mares-Carreño
jmaresc@ipn.mx

1 Electrical Engineering Department, CINVESTAV IPN, Av. Instituto Politécnico Nacional 2508, Gustavo A. Madero, San Pedro Zacatenco, 07360 Mexico City, Mexico

2 Unidad Profesional Interdisciplinaria de Ingeniería Campus Hidalgo, UPIIH IPN, Carretera Pachuca-Actopan Km 1+500, San Agustín Tlaxiaca, 42162 Hidalgo, Mexico

Several designs for MEMS micromotors have been proposed, based on different actuation principles such as piezoelectric (Srinivasa Rao et al. 2020), electromagnetic (Merzaghi et al. 2011; Chan et al. 2012; Getpreecharsawas et al. 2006; Frechette et al. 2001; Livermore et al. 2004), thermal (Khiat, et al. 2012) or ultrasound (Kaajakari and Lal 2007), however electrostatics has been the preferred method for MEMS micromotor actuation (Fan et al. 1989; Mehregany et al. 1990; Uranga et al. 2005; Tian et al. 2016; The 4th Annual IEEE International Conference on Nano/Micro Engineered and Molecular Systems; Basha et al. 2007; Zhang et al. 2005; Singh et al. 2006; Computer et al. 2013; Baginsky and Kostsov 2004; Favrat'), perhaps as it only needs an energy difference in pairs of misaligned and electrically energized plates in order to generate the motion of the rotor, which makes it easy to apply in the context of microelectronics, as the insertion of materials foreign to the processes of microelectronics is not necessary, as in the case of electromagnetically actuated motors where ferromagnetic materials are needed.

The design of electrostatically actuated MEMS micromotors allows the monolithic integration of the micromotor structure and the drive circuit, as both can be built in the same substrate (Horstmann and Goser 2003; Ericsson et al.

2023). Such monolithic MEMS are known as CMOS-MEMS and constitutes a basis for the development of intelligent sensors and actuators systems (Horstmann and Goser 2003), while reducing the setbacks of a hybrid integration of the micromotor structure and its drive circuit. In working with CMOS-MEMS the use of an FGMOS transistor as a transducer between an inertial parameter of a microstructure and an electrical signal has been demonstrated in Abarca-Jiménez et al. (2018); Abarca-Jiménez et al. 2019).

In this work, the design and simulation of an CMOS MEMS micromotor with electrostatic actuation is presented. The main goal of the design is to integrate monolithically the structure of the micromotor, along with a speed sensor based on a FGMOS transistor and the control circuit and lay the foundation for the development of monolithic closed-loop controlled micromotors.

2 Micromotor design

There are two types of micromotors: linear and angular or rotary (Khiat et al. 2012). This work concentrates on angular motors based on electrostatic actuation. Figure 1 shows the top view of an angular micromotor, the rotor (made up of a single piece), and the stator comprised of a conductive material.

The main parts that compose the proposed micromotor are the rotor, stator, bearing, shield, shaft, and cover generally made up of conductive materials, as shown in Fig. 2.

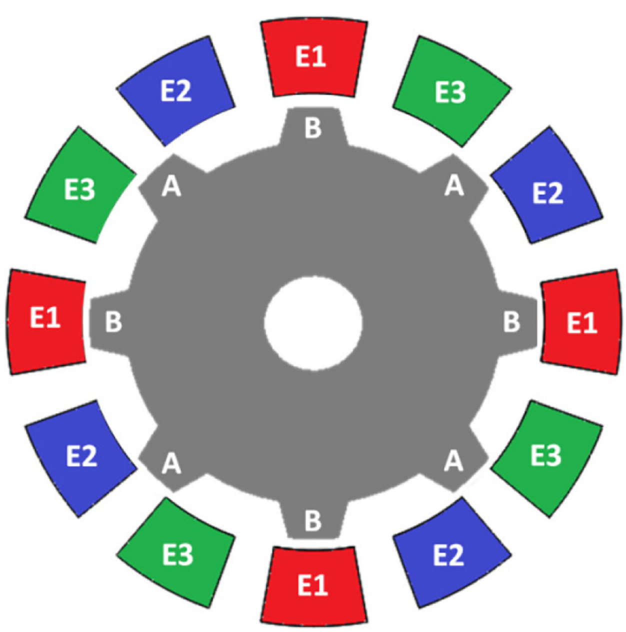

Fig. 1 The top view of an angular micromotor, the rotor (made up of a single piece), and the stator comprised of a conductive material

To optimize the performance of the micromotor, the geometric parameters considered were (see Fig. 3):

- Number of rotor poles (N_r)
- Number of stator poles (N_s)
- Rotor radius (r_0)
- Rotor tooth height (Δr)
- Rotor tooth shape
- Bearing radius (r_{Shaft})
- The gap between rotor and stator (d)
- The gap between bearing and rotor (r_{er})
- Rotor thickness (t)
- Shield radius (r_{Shield})
- Bearing diameter (d_c)

Since micromotors that work under the principle of electrostatic forces generally require an operating voltage greater than 15 V, as shown in Basha et al. 2007 and (Sarajlic et al. 2010), it is necessary to consider that their control circuit requires a type of power transistor to prevent p–n junction breakdown. Contrary to the previous point, this work proposes the design of a micromotor that allows operating at low voltages and, in turn, being compatible with CMOS-MEMS (Complementary Metal Oxide Semiconductor-Micro Electromechanical Systems) technology. The system is composed of an electrostatic motor and a transistor; the element that makes electromechanical interaction possible is the FGMOS.

3 The FGMOS

Figure 4 shows the structure of a floating gate MOS transistor (FGMOS). This is a conventional MOS transistor made up of the drain (D), the source (S), the substrate (B), and the gate (G). A second gate (CG) is added, making the gate electrically isolated. Thus, it is possible to assume that the gate remains floating, giving the floating gate (FG) its name.

Figure 5 represents the equivalent circuit of the parasitic capacitances of the FGMOS transistor. Cc is the capacitance formed by the control gate and the floating gate. This capacitor will be used for the mechanical coupling between the control circuit and the micromotor; for this reason, it will be called the sensing capacitor from now on. C_D is the parasitic capacitance due to the overlap between the floating gate and the drain; C_S is the parasitic capacitance due to the overlap between the floating gate and the source; finally, C_{OX} is the capacitance between the floating gate and the substrate.

For the analysis of the operation of the FGMOS, consider V_o and V_{DS} as the voltage source connected to control gate and drain, respectively, assuming an N-type transistor,

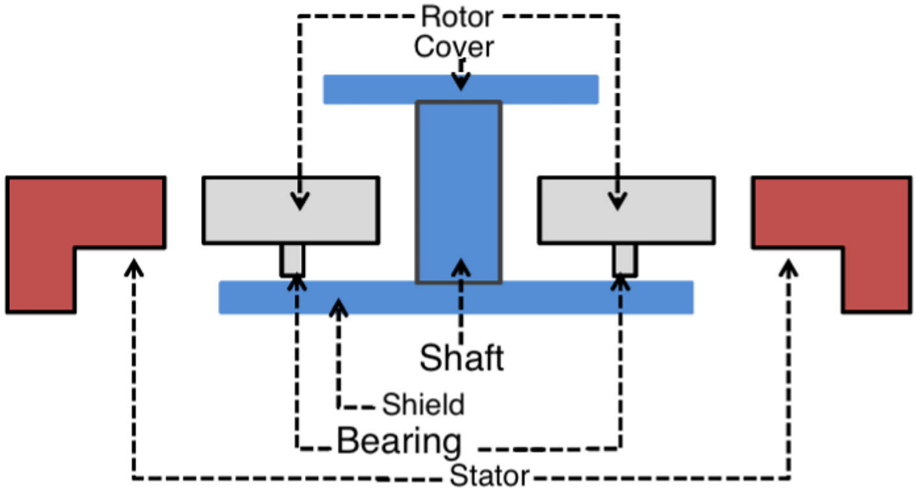

Fig. 2 Cross-section of a micromotor, the main parts are shown

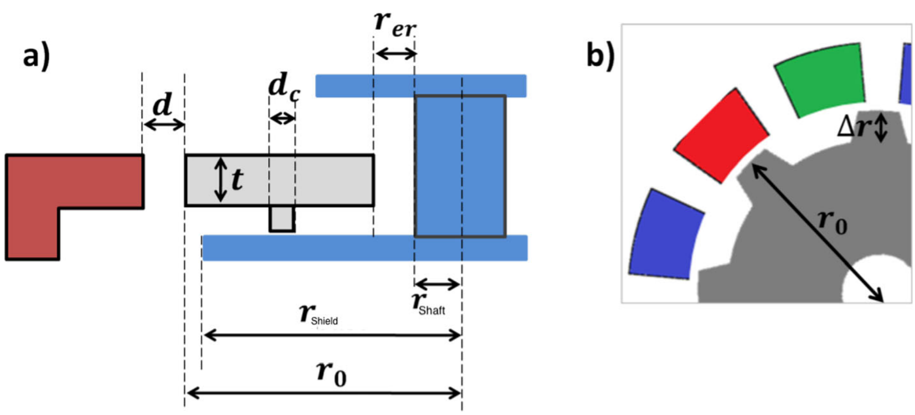

Fig. 3 View of a section of a micromotor, **a** Cross section and **b** Flat view

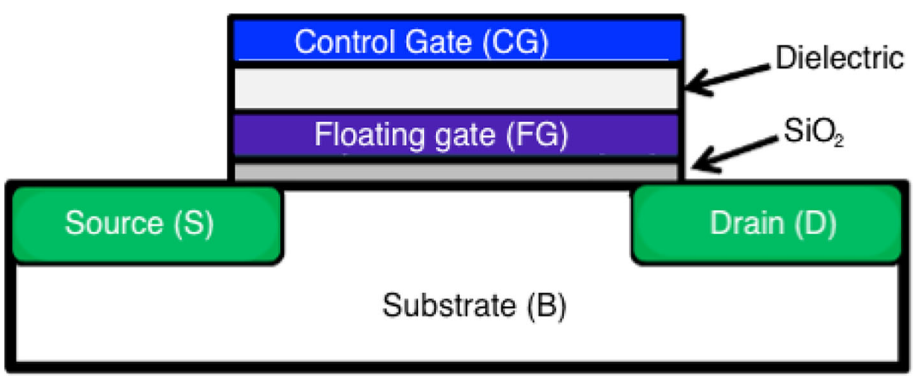

Fig. 4 Cross section of a FGMOS transistor

with the substrate and the source both connected to ground. The equivalent circuit remains as show in Fig. 6.

Denote the voltage across the floating gate V_{FG} as follows (see Eq. 1 and Eq. 2):

$$V_{FG} = \frac{C_C}{C_{TOT}} V_o + \frac{C_D}{C_{TOT}} V_{DS} \tag{1}$$

$$C_{TOT} = C_C + C_D + C_S + C_{OX} \tag{2}$$

A minimal value is assumed for $\frac{C_D}{C_{TOT}}$, resulting in an approximate value of V_{FG} as (see Eq. 3):

$$V_{FG} \approx \frac{Cc}{C_{TOT}} V_o = K_{CG} V_o \tag{3}$$

The term $K_{CG} = Cc/C_{TOT}$ is denoted as a variable coupling coefficient and will be the parameter controlling the current in the drain I_{DS} of the transistor since C_C can be mechanically modulated while all the other terms are fixed. Thus, the drain current of the FGMOS can be expressed as follows (see Eq. 4):

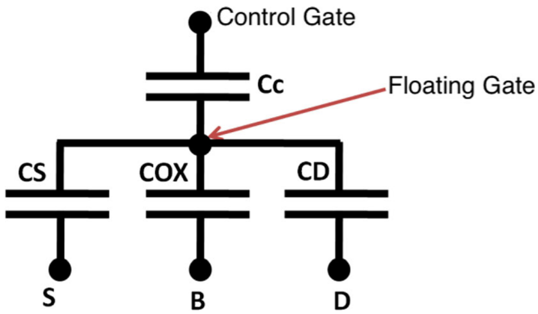

Fig. 5 Simplified equivalent circuit of the capacitance of an FGMOS

$$I_{DS} = \frac{\mu_n C_{OX} W}{L}\left(V_{FG} - V_{FB} - 2\varnothing_F - \frac{V_{DS}}{2}\right)V_{DS} + -\frac{2}{3}\mu_n\frac{W}{L}\sqrt{2\varepsilon_s q N_a}\left((2\varnothing_F + V_{DB})^{2/3} - (2\varnothing_F + V_{SB})^{2/3}\right) \quad (4)$$

where μ_n is the carrier mobility, W and L are the drawn channel width and length of the transistor, respectively, V_{FB} the flat–band voltage, $2\phi_F$ is the surface potential, V_{DS} is the drain–source voltage, ε_s is the semiconductor permittivity, q is the electron charge, N_a is the substrate impurity concentration, V_{DB} is the drain–bulk voltage and V_{SB} is the source–bulk voltage.

The sensing capacitor that makes up the coupling coefficient is a parallel plate capacitor present between the rotor and the stator, and it will be changing as the micromotor rotates, so it can be configured as a speed sensor.

4 General description of developing methodology

As already mentioned, this work follows the design based on design rules dictated by a CMOS silicon foundry to configure an FGMOS device. The variable capacitor (Cc) was included in the same chip. Also, as this technology offers neither bulk nor surface micromachining like that provided by MEMS dedicated technologies (like MEMSCAP, for instance), a post-process micromachining step can be added after the IC chip is received from MOSIS the same way it was done in Frechette et al. 2001. The system's design is at the core of this idea, so its shape and size follow the On-Semi design rules.

On the other side, from the electrical and mechanical point of view, the mass and shape of the micromotor and the electrical and inertial forces present are closely related. Friction force and electrostatic force must be unbalanced for the micromotor to move or stay stationary. For example, if you want the micromotor to move, the electrostatic force generated must be greater than the friction force; otherwise, if you want the micromotor to be static, the friction force must be more significant.

For this proposal, the rotor is made of aluminum and consists of two structural metal layers, together with the interconnection between them, called via layer. Besides, the stator comprises 5 layers: three structural metal layers, and two intermediates via layers (the technology here considered offers three metal layers and their respective interconnections). The central element is manufactured with five layers like the stator and fulfills the function of limiting unwanted rotor movements, considering the post-processing of surface micromachining required. Figure 7 and Fig. 8 show a micromotor cross-section.

Considering that N_r is the number of the poles of the motor, the volume is (see Eq. 5):

$$Vol = \left[\pi\left(r_1^2 - r_2^2\right) + N_r\left(\Delta r\frac{B+b}{2}\right)\right]t + \left[\pi\left(r_2^2 - r_3^2\right)\right]t_o \quad (5)$$

The morphological parameters listed in Table 1 optimally relate electromechanical performance and On-Semi manufacturing rules.

If the rotor is moving around the z-axis, then the friction force F_f is calculated as (see Eq. 6):

$$F_f = \mu\rho g Vol \quad (6)$$

Fig. 6 FGMOS **a** DC biasing of the transistor, **b** equivalent circuit

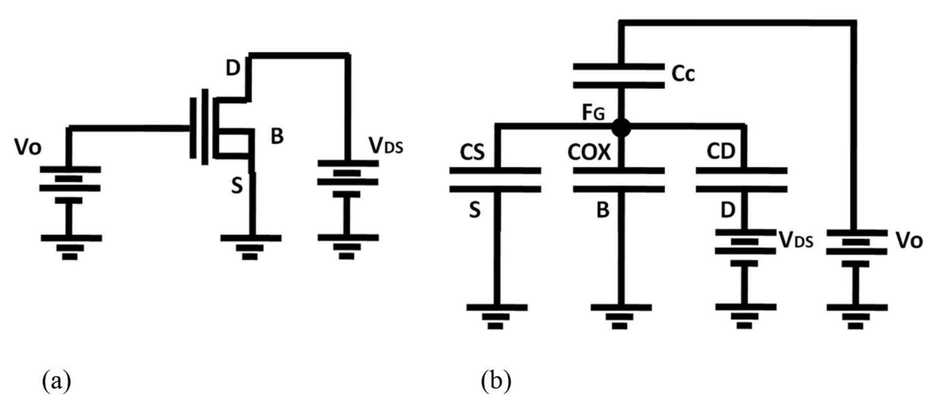

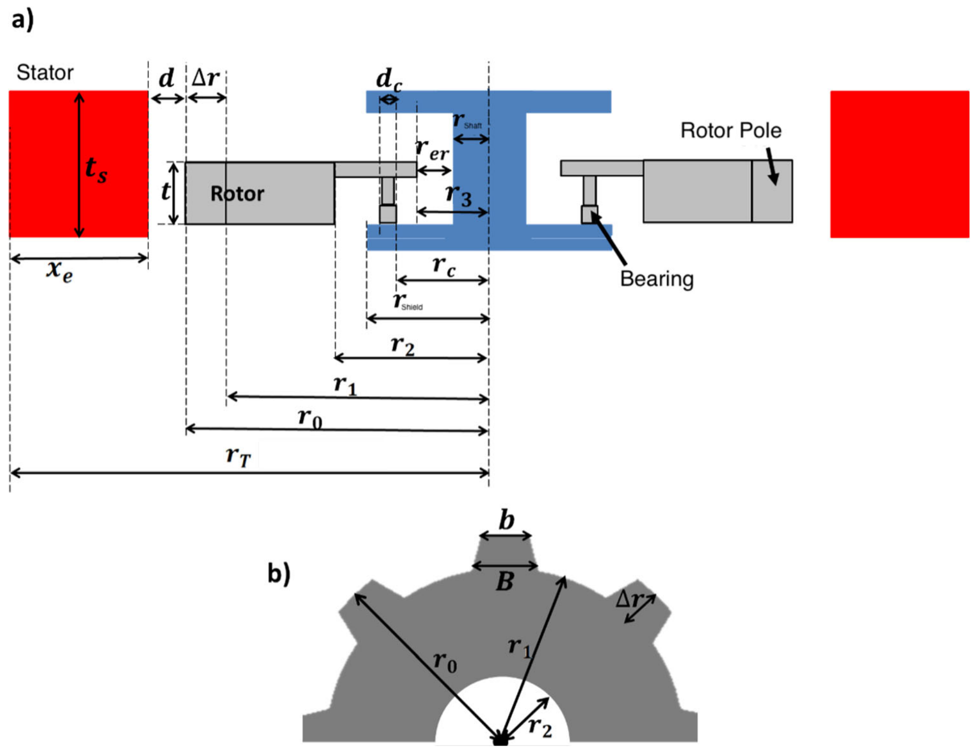

Fig. 7 Morphological parameters of the micromotor **a** a cross-section view, **b** rotor seen in detail

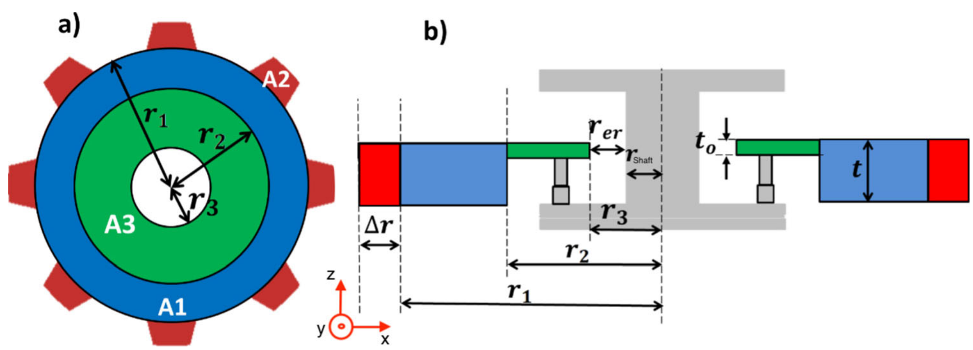

Fig. 8 Micromotor structure: **a** A1 y A3 has a toroid form, **b** a cross-section view

Table 1 Morphological parameters of the micromotor

Morphological parameter	Metrics
t	2.31 µm
r_1	200 µm
r_2	180 µm
N_r	50
Δr	18 µm
B	15 µm
b	9 µm
r_3	53 µm
t_o	0.57 µm
d	3.6 µm

Considering that g is the gravitational acceleration, ρ the density of material and μ is the static friction coefficient.

On the other hand, the electrostatic force on the rotor is (see Eq. 7):

$$F_e = N_s \varepsilon_r \varepsilon_o \frac{t}{2d} V_o^2 \tag{7}$$

Considering that N_s is the number of active stator poles, ε_r relative permittivity of the medium, ε_o is the permittivity of vacuum and V_o is the micromotor driving voltage. The stator has 75 poles, which are activated only in groups of 50 at a time, to establish a geometric relationship between rotor and stator poles of 2/3 as shown in Basha et al. 2007 and (Otani et al. 2006).

Considering the metrics in Table 1 and that the mechanism is composed of layers of aluminum surrounded by

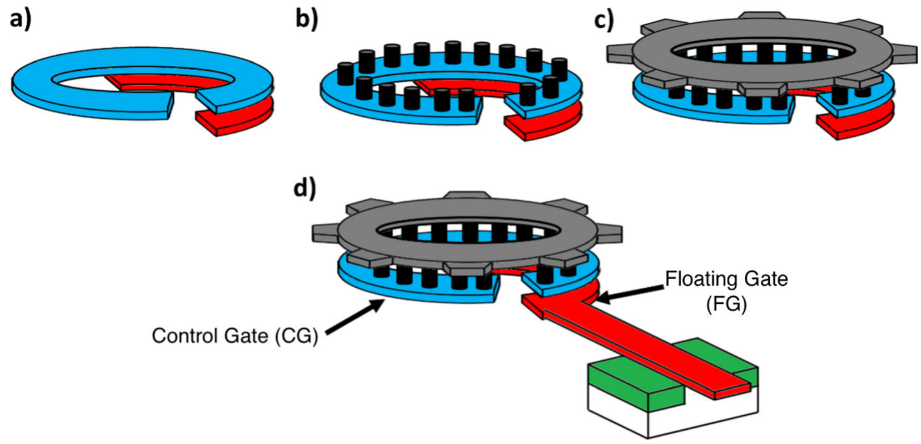

Fig. 9 **a** Capacitor Cc **b** Metal contacts between CG y FG (*Metal1*) **c** The CG plate connected through the metal contacts to the rotor (*Metal2*) **d** the FG plate extends and forms the floating gate of the FGMOS

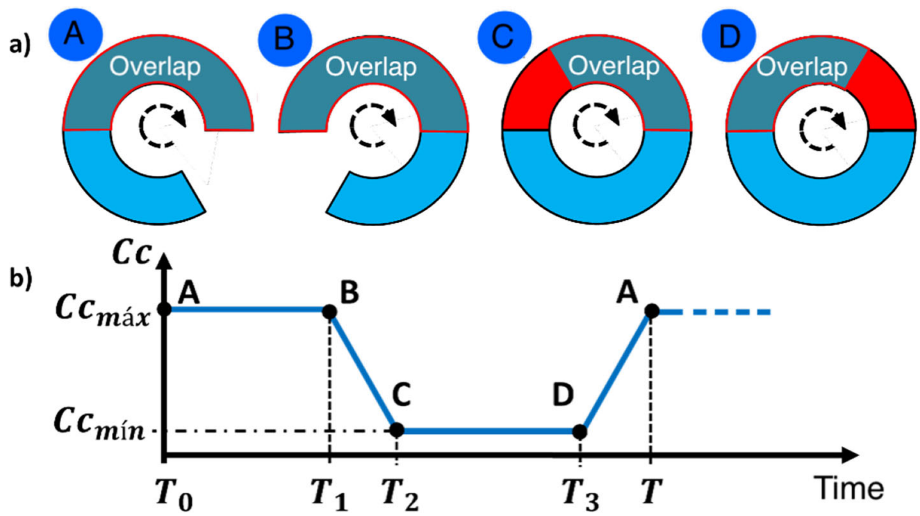

Fig. 10 **a** Turning the micromotor clockwise **b** Variation of the capacitance when the motor is turning clockwise

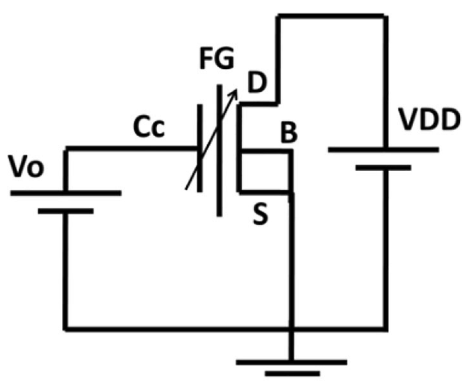

Fig. 11 Schematic circuit of the FGMOS connections

air, the relationship between the inertial force and the electrostatic force is as follows (see Eq. 8):

$$\frac{A}{B}\mu < V_o^2 \tag{8}$$

Considering $A = \rho g Vol$ and $B = N_s \varepsilon_r \varepsilon_o \frac{t}{2d}$. Then, for the motor to move, the friction force F_f must be less than the electrostatic forceF_e. The unknown variables are the coefficient of static friction μ and the activation voltage V_o because the On-Semi rules and the designer determine the morphology. In this case, the coefficient of static friction to consider is the one present between the upper aluminum layer and the lower aluminum layer, which is the area where the rotor bearings and the rotor base come into contact (see Fig. 8). However, the value to be considered is uncertain for several reasons: the post-micromachining process, the possible drop effect, the roughness of the resulting surface, and the scarce experimental data are very difficult to be known and measured. However, to take this coefficient into account, it is suggested to give the static friction coefficient a value between 1 and 3 because, as reported in Vinhais et al. (2006) and (Reddy et al. 2018), it is sufficient to establish a high friction coefficient. On the other hand, under the previous considerations, the voltage necessary to drive the micromotor satisfies the condition that:

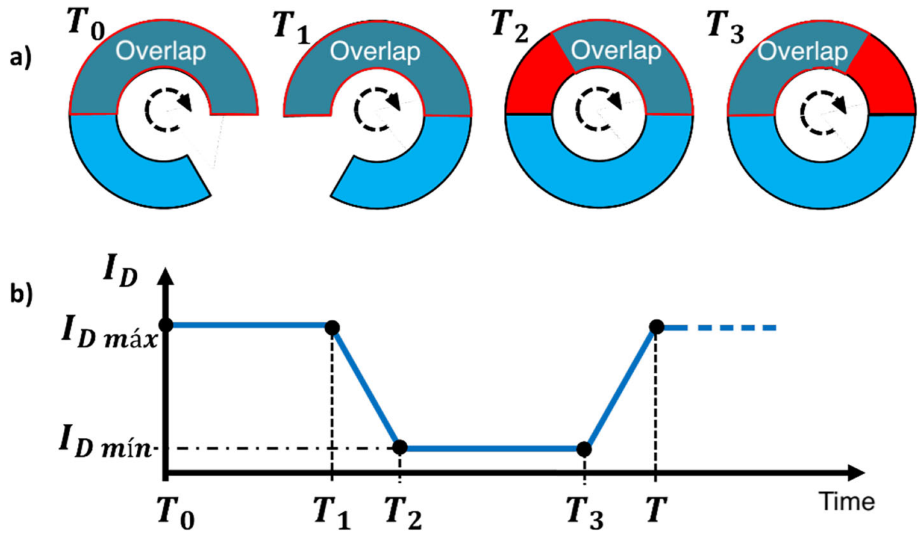

Fig. 12 **a** Turning the micromotor clockwise. **b** Variation of the current drain I_{DS} when the motor is turning clockwise

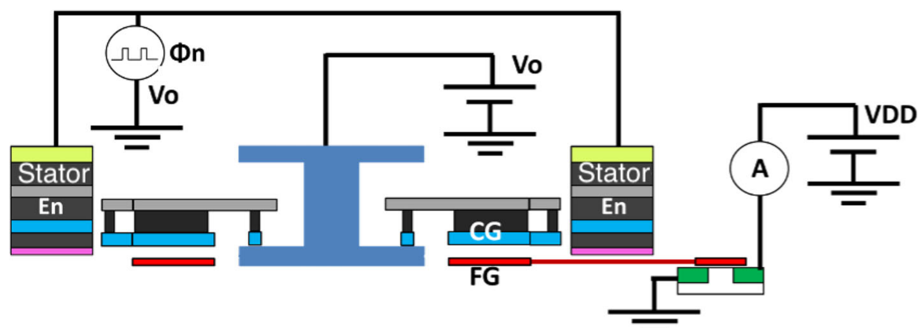

Fig. 13 Diagram of the cross-section of the micromotor and the structure of the capacitor Cc coupled to the rotor, formed with the layers of On-Semi 0.5micron CMOS technology

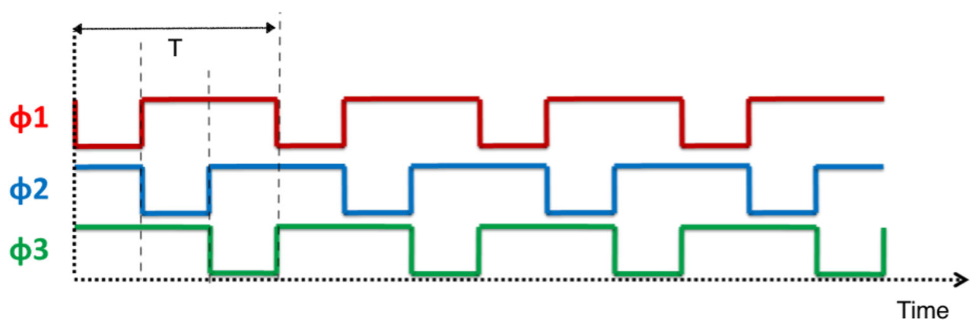

Fig. 14 Signals applied to the stator, considering a period T, each signal duration 1/3 of a period

$$\begin{aligned} &\mu = 1, V_o > 4.98V \\ &\mu = 2, V_o > 7.04V \\ &\mu = 3, V_o > 8.63V \end{aligned} \tag{9}$$

5 The speed sensor and the FGMOS

Next, an explanation of the way the sensor is configured based on the FGMOS, follows. As was explained before, there is a fixed plate being part of the sensing capacitor C_C, which corresponds to the floating gate (FG) of the FGMOS transistor, and a moving plate mechanically coupled to the rotor, whose node corresponds to the control gate (CG). The first plate of the capacitor is made of polysilicon (*Poly1*), and the second plate is made of metal (*Metal1*). Both layers are available in On-Semi 0.5 µm technology. The shape of the proposed capacitor plates is that of a flat semi toroid since it does not interfere with the rotation. An angle value of 180° is proposed for the FG plate, while for the CG plate, an angle of 300° is established. With these defined angles, no matter how much the rotor turns, the capacitors are always overlapping by at least 120° (see Fig. 9).

.

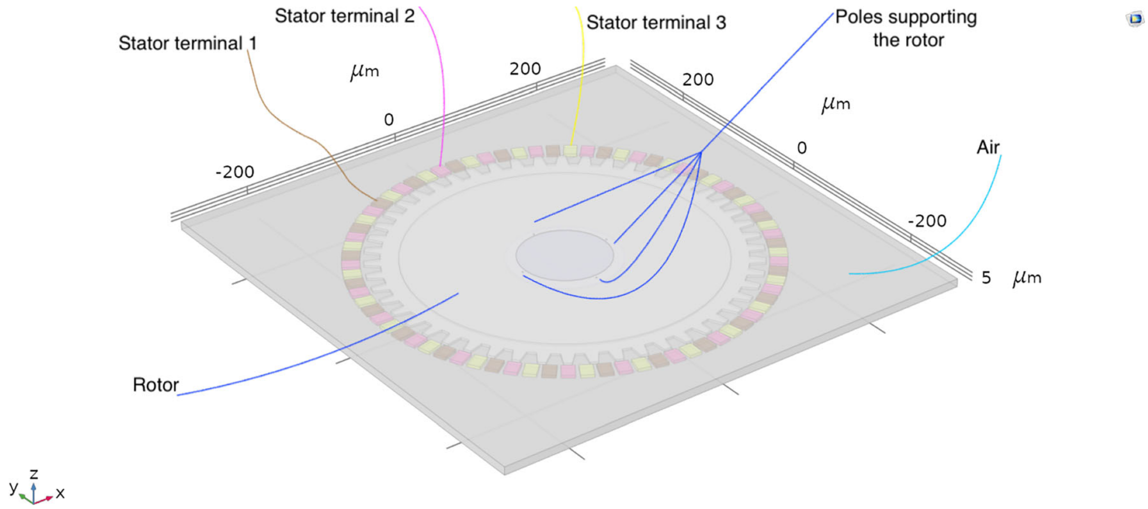

Fig. 15 Simulated micromotor model in multiphysics software to determine axial torque

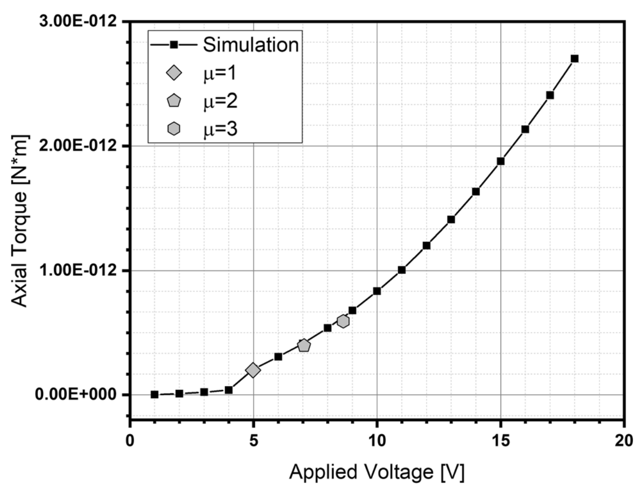

Fig. 16 Simulation results, applying a variable voltage on the stator and rotor at the same time

If the rotor turns, plates CG and FG overlap differently for different situations, causing the capacitance C_C to change, as shown in Fig. 10.

$$Cc_{máx-min} = \frac{A_{máx-min}\varepsilon_{air}\varepsilon_o}{d} = \frac{\frac{\theta_{máx-min}}{2}\left(r_1^2 - r_2^2\right)\varepsilon_{air}\varepsilon_o}{d} \tag{10}$$

Figure 11 shows the equivalent circuit of the FGMOS, the speed sensor, and the micromotor.

If the value of C_C changes, the coupling coefficient K_{CG} changes, which in turn changes the drain current I_{DS} (see Fig. 12).

Figure 13 shows a cross-section of the structure of the micromotor, detailing each of the layers of On-Semi's CMOS technology. Furthermore, it is possible to observe the activation voltage (V_0) of the rotor and stator, the activation voltage of the drain (V_D), and their variation in

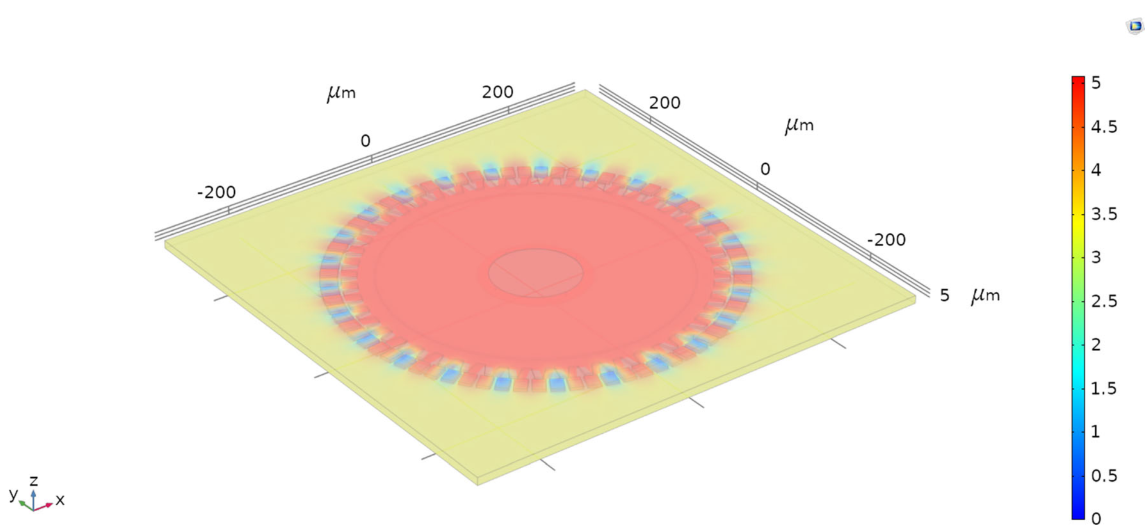

Fig. 17 Voltage applied to the micromotor; example is shown when using a maximum voltage signal of 5 V

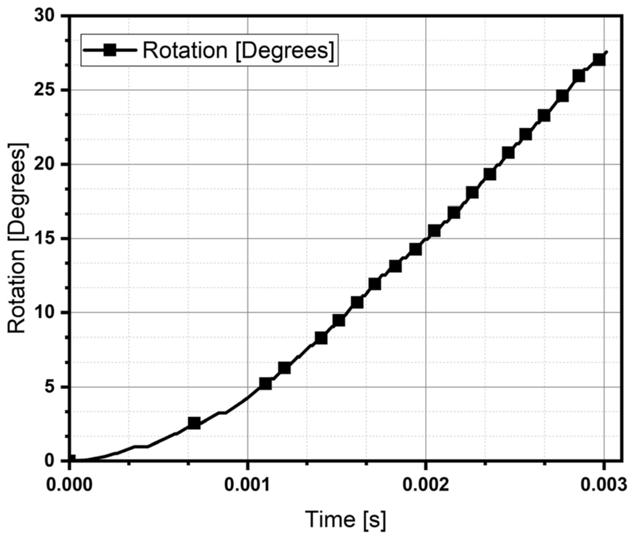

Fig. 18 Angular displacement of the rotor over 3 ms, with a positive 18 V voltage applied

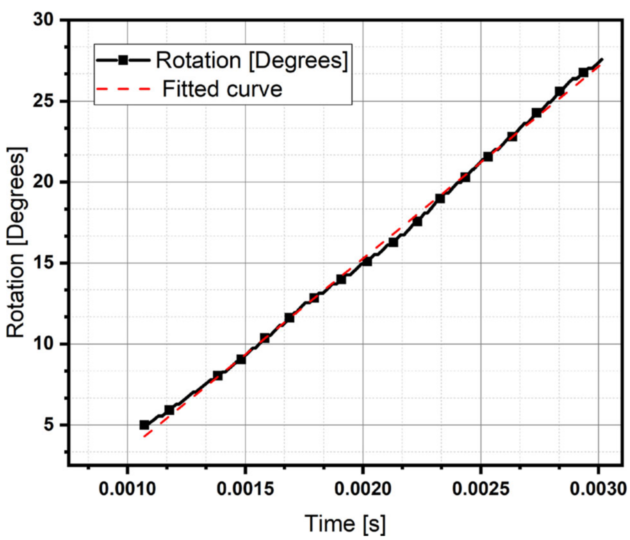

Fig. 19 Curve fit over the steady part of the response of the micromotor

current (I_{DS}). The layers of Poly2, Metal 1, Metal 2, and Metal 3, with their respective trajectory between layer and layer, make up the stator and the central body. While the rotor only requires metal 1 and 2. The layer of Poly 1 is used only for the sensor, which is, in turn, the floating gate of the transistor. The stator must be wider than the rotor to avoid that the effective area of overlap decreases due to misalignments when rotating.

To drive the motor, it is necessary to generate the alternating signals applied to the stator; in general, keeping the stator in a high state except for the set that drives the rotor through electrostatic force. To advance clockwise, the order of the signals ϕ_1, ϕ_2 and ϕ_3 are followed, Fig. 14, considering that the stator is divided into three sets as was

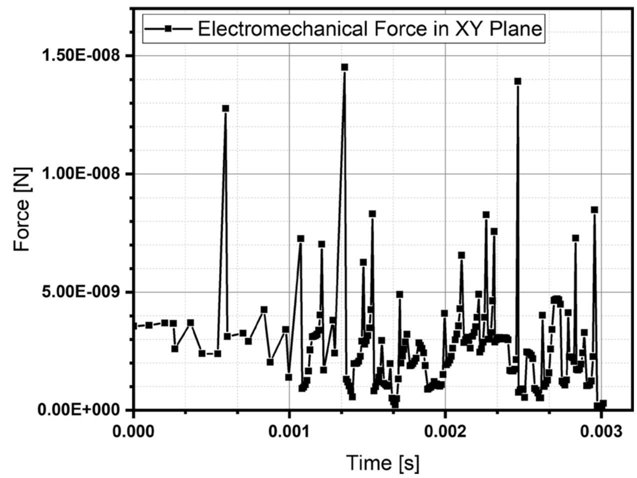

Fig. 20 Electrostatic force on the rotor, with a positive 18 V voltage applied

shown in Fig. 1, and the voltage signals are associated E1-ϕ_1, E2-ϕ_2, and E3-ϕ_3.

6 Simulations and results

Static and time-dependent simulations were made in COMSOL Multiphysics. For both simulations there are 2 physics to be solved for: Solid mechanics and Electrostatics along with a Multiphysics coupling for the electromechanical forces. The rotor has a continuous signal, while the stator is powered, as shown in Fig. 15; the voltage for all terminals varies from 1 to 18 V, and the purpose is to calculate the axial torque. The theoretical axial torque is compared with the simulated to verify the design. The friction force is obtained using the rotor's mass, the value of the coefficient of friction, and the gravitational acceleration. A parametric sweep on the voltage is made to calculate the axial torque and compare it against the friction force in the static simulation.

The static simulation considers the following factors, Fig. 15 and Fig. 16:

- There is a contact pair between the elements that support the rotor and the substrate on which it lies.
- The voltage ranges from 1 to 18 V.
- The rotor of the micromotor is limited to rotate only about the z-axis by adding a rigid connector that determines the degrees of freedom.
- The gravitational acceleration is parallel to the axis of the motor, whose direction is towards the substrate.
- The rotor has a positive voltage applied all the time.

- The multiphysics coupling of the system is achieved by adding electromechanical force calculation.

The expected axial torque for different values of friction coefficients coincides with the simulated axial torque values, see Fig. 16. Note that the simulation results depend only on the applied voltage values.

For the time dependent simulation, in addition to the Solid mechanics, Electrostatics and the Multiphysics coupling, the Events and Moving Mesh interfaces are also solved. This simulation allows observing the dynamics of the micromotor and has the following conditions (some guidelines used are based on (Meng et al. Apr. 2009) and (Yang et al. 2004)):

- The stator is fed with three signals, as shown in Fig. 15 and Fig. 16, with a frequency of 500 Hz.
- Applied voltage is 18 V.
- Total time of the simulation is 3 ms.
- The mesh of the air domain surrounding the rotor and the stator, is defined as a moving mesh.
- A stop condition based on the distortion of the mobile mesh is used.
- The study consists of several solution steps, where the number of steps depends on the tightness of the stop condition.
- When the stop condition is reached, the domains are remeshed based on the spatial displacement calculated for the moving mesh. The remeshing allows keeping good quality elements and avoiding convergence issues (Fig. 17).

The results obtained include angular displacement of the rotor and the electrostatic force necessary to carry out the movement of the micromotor. The rotation of the micromotor reaches 28° in 0.003 s. From Fig. 18, it is possible to observe that the movement of the micromotor is nonlinear from 0 s to 0.001 s this is attributed to the fact that the simulation starts from an initial state of rest, consequently it can be concluded that the behavior of the micromotor during this period can be interpreted as the transient of the response.

In the time from 0.001 s to 0.003 s the response is almost linear (Fig. 18), and it can be regarded as the steady state of the response. Over the steady part of the response a curve fit was made (Fig. 19), from which a linear function (Eq. 11) was obtained.

From Eq. 11, it can be computed the expected time for the rotor to complete a full revolution which is 0.0311 s, given this time the angular velocity of the micromotor will be 64.32 rad/s at 500 Hz of input frequency.

$$y = 11848.801x - 8.416 \tag{11}$$

In Fig. 20 the graph of the magnitude of the electromechanical force in the XY plane is shown, proving that the electrostatic force maintains sufficient magnitude in order to produce the angular movement of the rotor. It is essential to highlight that the lack of smoothness of the force graph obtained is due to the limited number of points taken from the solver during the solution and because of the nature of the micromotor, as the exerted electromechanical force depends on the relative movement between the rotor and stator.

7 Conclusions

The designed micromotor is compatible with CMOS technology and with the operating voltage of embedded systems technology because the voltages necessary to break the inertia of the micromotor are reached from 4.8 V considering values of unit friction coefficients, reaching up to 8.63 V with friction coefficient 3. These values can be considered manageable in embedded systems such as MEMS since power elements are not required to design digital circuits to control them. The linear movement of the micromotor allows establishing a quadratic relationship in the change of the electric current of the FGMOS transistor since the capacitance generated between the rotor and the moving sensor changes concerning the overlap area. Since the micromotor is surrounded by air, the time-dependent simulations of the system require long computation times. There are four physics involved: Solid Mechanics, Electrostatics, Events, and Moving mesh in addition to the electromechanical forces coupling. Finally, the angular displacement obtained from the simulation shows a linear behavior as expected from the design.

Acknowledgements The authors acknowledge SIP-IPN (Grant 20241962 and 20241688) and Unidad Profesional Interdisciplinaria de Ingeniería Campus Hidalgo- Instituto Politécnico Nacional for their support.

Data availability Not applicable.

References

Abarca-Jiménez GS et al (2018) Inertial sensing MEMS device using a floating-gate MOS transistor as transducer by means of modifying the capacitance associated to the floating gate. Microsyst Technol 24(6):2753–2764. https://doi.org/10.1007/s00542-017-3647-7

Abarca-Jiménez GS et al (2019) Validation of a CMOS-MEMS accelerometer based on FGMOS transduction by electromechanical modification of its coupling coefficient. Microsyst Technol 25(11):4163–4171. https://doi.org/10.1007/s00542-019-04375-6

Annual IEEE Computer Conference, IEEE regional symposium on micro and nanoelectronics 2013.09.25-27 Langkawi, IEEE regional symposium on micro and nano electronics 2013.09.25-27 Langkawi, and RSM 2013.09.25-27 Langkawi, 2013 IEEE Regional Symposium on Micro and Nanoelectronics (RSM) 25-27 Sept. 2013, Holiday Villa Beach Resort & Spa, Langkawi, Malaysia

Baginsky IL, Kostsov EG (2004) Electrostatic micromotor based on ferroelectric ceramics. J Micromech Microeng 14(11):1569–1575. https://doi.org/10.1088/0960-1317/14/11/019

Basha MA, Safavi-Naeini S, Chaudhuri SK (2007) Design and fabrication of an electrostatic micromotor with a low operating voltage. In: TRANSDUCERS 2007 - 2007 International Solid-State Sensors, Actuators and Microsystems Conference, Lyon, France, pp 1139–1142. https://doi.org/10.1109/SENSOR.2007.4300336

Chan ML et al (2012) Design and characterization of MEMS micromotor supported on low friction liquid bearing. Sens Actuators A Phys 177:1–9. https://doi.org/10.1016/j.sna.2011.08.003

Chen X, Cui DF, Zhang LL (2009) Design and fabrication of microfluidic chip with micro/nano structures. In: 2009 4th IEEE International conference on nano/micro engineered and molecular systems, Shenzhen, China, pp 98–101. https://doi.org/10.1109/NEMS.2009.5068535

Ericsson P, Hedstrom M, Olsson A, Scholes A, Svennebrink J, Vieider C, Wenk B (2003) MEMS switches and other RF components fabricated using CMOS postprocess compatible surface micromachining. In: TRANSDUCERS'03. 12th International conference on solid-state sensors, actuators and microsystems. Digest of Technical Papers (Cat. No. 03TH8664), Vol. 1, pp 895–898. https://doi.org/10.1109/SENSOR.2003.1215619

Yu-Chong T, Muller RS (1990) Frictional study of IC-processed micromotors. Sens Actuators A Phys 21(1–3):180–183. https://doi.org/10.1016/0924-4247(90)85034-2

Favrat P, Paratte L, Ballan H, Declercq MJ, de Rooij NF (1997) A 1.5-V-supplied CMOS ASIC for the actuation of an electrostatic micromotor. In: IEEE/ASME Transactions on Mechatronics 2(3):153–160. https://doi.org/10.1109/3516.622967

Frechette LG, Nagle SF, Ghodssi R, Umans SD, Schmidt MA, Lang JH (2001) An electrostatic induction micromotor supported on gas-lubricated bearings. In: Technical Digest. MEMS 2001. 14th IEEE International Conference on Micro Electro Mechanical Systems, Interlaken, Switzerland, pp 290–293. https://doi.org/10.1109/MEMSYS.2001.906535

Getpreecharsawas J, Puchades I, Hournbuckle B, Fuller L, Pearson R, Lyshevski S (2006) An Electromagnetic MEMS Actuator for Micropumps. In: Proceedings of the 2nd International conference on perspective technologies and methods in mems design, Lviv, Ukraine, pp 11–14. https://doi.org/10.1109/MEMSTECH.2006.288652

Horstmann JT, Goser KF (2003) Monolithic integration of a silicon micromotor in combination with the CMOS drive circuit on one chip. Microelectron Eng. https://doi.org/10.1016/S0167-9317(03)00094-7

Kaajakari V, Lal A (2007) Micromachined ultrasonic motor based on parametric polycrystalline silicon plate excitation. Sens Actuators A Phys 137(1):120–128. https://doi.org/10.1016/j.sna.2007.01.020

Khiat A et al (2012) Linear and rotational thermal micro-stepper motors. Microelectron Eng. https://doi.org/10.1016/j.mee.2012.07.086

Livermore C, Forte AR, Lyszczarz T, Umans SD, Ayon AA, Lang JH (2004) A high-power MEMS electric induction motor. J Microelectromech Syst 13(3):465–471. https://doi.org/10.1109/JMEMS.2004.828736

Mehregany M, Bart SF, Tavrow LS, Lang JH, Senturia SD, Schlecht MF (1990) A study of three microfabricated variable-capacitance motors. Sens Actuators A Phys 21(1–3):173–179. https://doi.org/10.1016/0924-4247(90)85033-Z

Meng G, Zhang WM, Huang H, Li HG, Chen D (2009) Micro-rotor dynamics for micro-electro-mechanical systems (MEMS). Chaos Solitons Fractals 40(2):538–562. https://doi.org/10.1016/j.chaos.2007.08.003

Merzaghi S, Koechli C, Perriard Y (2011) Development of a hybrid MEMS BLDC micromotor. IEEE Trans Ind Appl 47(1):3–11. https://doi.org/10.1109/TIA.2010.2090841

Y. Otani and F. Janabi-Sharifi, Eds., SPIE, Oct. 2006, p. 63740C. doi: https://doi.org/10.1117/12.687698.

Reddy RR, Okamoto Y, Mita Y (2018) An on-chip test structure for studying the frictional behavior of deep-RIE MEMS sidewall surfaces. In 2018 IEEE international conference on microelectronic test structures (ICMTS), IEEE, pp 173–178. https://doi.org/10.1109/ICMTS.2018.8383792

Sarajlic E, Yamahata C, Cordero M, Fujita H (2010) Three-phase electrostatic rotary stepper micromotor with a flexural pivot bearing. J Microelectromech Syst 19(2):338–349. https://doi.org/10.1109/JMEMS.2010.2040139

Singh J, Agarwal A, Soundarapandian M (2006) A novel electrostatic microactuator for large deflections in MEMS applications. Thin Solid Films. https://doi.org/10.1016/j.tsf.2005.09.041

Srinivasa Rao K, Hamza M, Ashok Kumar P, Girija SK (2020) Design and optimization of MEMS based piezoelectric actuator for drug delivery systems. Microsyst Technol 26(5):1671–1679. https://doi.org/10.1007/s00542-019-04712-9

Tian WC, Chen ZQ, Cao YR (2016) Analysis and test of a new MEMS micro-actuator. Microsyst Technol 22(5):943–952. https://doi.org/10.1007/s00542-015-2802-2

Uranga A et al (2005) Fully CMOS integrated low voltage 100 MHz MEMS resonator. Electron Lett 41(24):1327–1328. https://doi.org/10.1049/el:20053473

Vinhais HF, de Godoy PH, Silva EC (2006) Optimized design of an electrostatic side-drive micromotor. ABCM Symposium Series in Mechatronics 2:433–450

Yang JP, Chai J, Lu Y (2004) Dynamics simulation of MEMS device embedded hard disk drive systems. Microsyst Technol 10(2):115–120. https://doi.org/10.1007/s00542-003-0310-2

Zhang W, Meng G, Li H (2005) Electrostatic micromotor and its reliability. Microelectron Reliab 45(7–8):1230–1242. https://doi.org/10.1016/j.microrel.2004.12.017

Publisher's Note Springer Nature remains neutral with regard to jurisdictional claims in published maps and institutional affiliations.

Springer Nature or its licensor (e.g. a society or other partner) holds exclusive rights to this article under a publishing agreement with the author(s) or other rightsholder(s); author self-archiving of the accepted manuscript version of this article is solely governed by the terms of such publishing agreement and applicable law.